Design and Simulation of a Surface Wave-Based Cylindrical Hollow Plasma Cavity for Wakefield Booster for Future e^+e^- Colliders

Q. Luo, *Member, IEEE,* A. L. Zhang , and H. P. Peng

***Abstract*— A cylindrical hollow plasma cavity was designed for a particle-driven plasma accelerator experiment for future e^+e^- colliders. Surface wave ionization was used to generate a high-density, highly stable cylindrical hollow plasma instead of the laser ionization. Microwave and plasma models were used to optimize the plasma cavity structure, the gas pressure, and the microwave frequency and power to produce a high-quality plasma. The plasma simulation results show that with a 6 GHz at 2 kW microwaves power, a 100 mm × 400 mm (length) × 30 mm (thickness) hollow plasma column with a density of $2.76 \times 10^{15}/cm^3$ will be obtained. The fluctuations of the plasma density in longitudinal direction are less than 2%, which is satisfactory to provide a long and stable enough plasma region for the wakefield acceleration experiment. The details will be described in this article.**

***Index Terms*— Accelerator cavities, ionization chambers, plasma applications.**

I. Introduction

A NEW generation electron–positron collider—the Super Tau-Charm Facility (STCF)—has been proposed in China [1]. The STCF will have a luminosity exceeding 1×10^{35} cm^{-2} s^{-1} and a center-of-mass energy region of 2–7 GeV. This facility is extremely scientifically and strategically important for basic research as well as for the production of emerging technologies and the cultivation of extensive knowledge. Polarized electron and positron beams are needed to increase the capabilities of the STCF in China. The Linac of STCF can only provide a 3.5-GeV electron beam, however, to get a high-quality high-density positron beam, a higher electron energy is needed for the electron–target positron source. On the other hand, positron polarization is one of the most important upgrade plans for STCF in the future. The helical-undulator-based positron source recognized as the most feasible method for high density positron polarization, however, it need a very high energy electron beam [2] which is difficult to achieved by traditional high-energy accelerators.

Manuscript received March 13, 2021; revised April 19, 2021; accepted May 8, 2021. Date of publication May 25, 2021; date of current version June 10, 2021. This work was supported by the National Natural Science Foundation of China under Grant U1832169. The review of this article was arranged by Senior Editor C. A. Ekdahl. *(Corresponding author: A. L. Zhang.)*

Q. Luo is with National Synchrotron Radiation Laboratory (NSRL), University of Science and Technology of China, Hefei 230026, China (e-mail: luoqing@ustc.edu.cn).

A. L. Zhang and H. P. Peng are with the Department of Modern Physics, University of Science and Technology of China, Hefei 230026, China (e-mail: ailinz@ustc.edu.cn; penghp@ustc.edu.cn).

Color versions of one or more figures in this article are available at https://doi.org/10.1109/TPS.2021.3079509.

Digital Object Identifier 10.1109/TPS.2021.3079509

Plasma-based accelerators have higher (by more than three orders of magnitude) acceleration gradients than traditional accelerators and are therefore promising candidates for more compact particle accelerators in proof-of-concept experiments. In particular, the plasma wakefield accelerator (PWFA) at the Stanford Linear Accelerator Center (SLAC) has recently achieved gradients up to 100 GeV/m, enabling energy doubling of 42-GeV electrons in an 85-cm-long plasma electron source [3]. If the electron energy of STCF doubled to 7 GeV, the positron yield will be tripled due to the positron yield calculation. However, the beam ions accelerated by the plasma wakefield are subjected to intense transverse forces that can affect the efficiency of beam acceleration. Plasma hollow channels have been proposed as a means of producing field acceleration without the use of transverse forces [4].

Hollow plasma has been recognized to be capable of mitigating the beam output degradation, although it was originally suggested to confine the lasers [5]. For a hollow tube, an electron- and ion-free accelerating area with zero transverse forces is possible, which benefits the protection of the beam emittance [4]. Earlier experimental observations of hollow plasma channels based primarily on low-amplitude waves and linear plasma responses [7]–[14], as well as laser [7]–[11] or electron [12]. Positively charged drivers have fewer studies [6], [13]–[15], but this setup has a strong positron acceleration regime [15]. An experiment [16] created a 25-cm-long hollow channel. This opens up prospects for practical applications of hollow channels in plasma wakefield acceleration.

Particle-driven plasma accelerators generally need longer (by up to a meter) distance and lower (n_e 10^{14}–10^{18} cm^{-3}) plasma densities than laser-driven accelerators. An auxiliary laser may be needed to ionize the source species in a PWFA, because the electric fields of the driver may be too low for field ionization. Plasma sources play a central role in both laser- and particle-beam-based plasma accelerators, and the continued development of plasma sources is critical for applications based on plasma accelerators. The production of plasma sources should also be prioritized by research councils. A stable and reliable plasma source inspired by surface waves was designed and simulated in this study.

The electric field around surface waves propagating along a dielectric–plasma interface generates and sustains a surface wave plasma (SWP). An SWP source is a potential large-scale plasma-processing platform and has received increasing attention since the 1990s, with the rapid production of ultralarge-scale integrated devices, such as solar cells, flat panel displays,

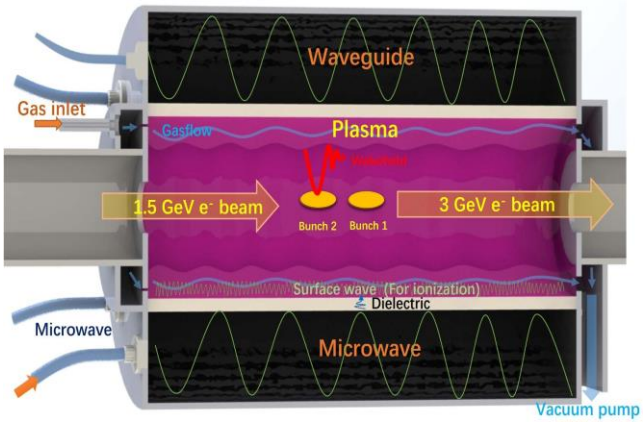

Fig. 1. Wakefield-multiplier positron source for STCF in China.

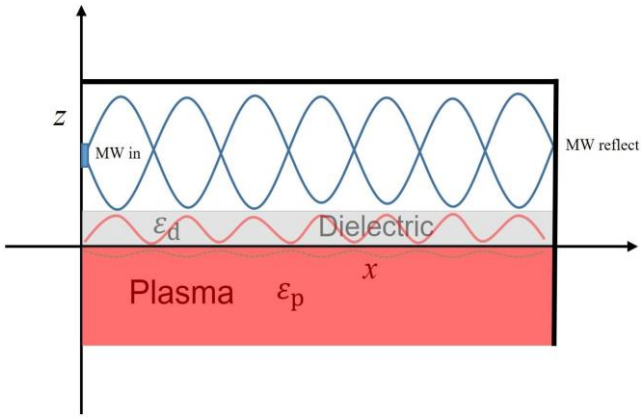

Fig. 2. Electromagnetic transmission in SPPs.

and microelectromechanical systems [17]. An SWP source offers many advantages over traditional plasma devices, such as the absence of electrodes and external magnetic fields that facilitate the production of large-scale, high-density, and uniform plasmas. The complex structure of an SWP source results in a complicated coupling between the coaxial cables, surface waves, and the plasma; thus, numerical simulations are urgently required to analyze related physical issues and optimize the cylindrical hollow plasma cavity system.

II. Physical Design of the Cylindrical Hollow Plasma Cavity

The cylindrical hollow plasma wakefield booster under design is shown in Fig. 1. In order to get an enough wakefield, the density hollow plasma should be more than $2\times 10^{15}/\text{cm}^3$. An electron driver beam and a hollow plasma channel are used as an accelerating structure. A driver beam drives a wakefield in a hollow plasma and accelerates the trailing beam behind the driver beam. A portion of the energy lost to the plasma can be used to accelerate the trailing beam. To get the high-quality high-density cylindrical hollow plasma for wakefield booster experiment, the cylindrical hollow SWP plasma source had been designed and simulated. To ensure the uniformity of the plasma density in the circumference direction, eight coaxial microwave feedings are used to supply microwave power to the cylindrical hollow plasma cavity. The optimized dimensions (from a rectangular surface experiment and the microwave, plasma simulation) of the cylindrical hollow plasma cavity are $\varnothing 320$ mm $\times$ 400 mm. The waveguide length is designed to transport a stationary wave along the waveguide (depending on the microwave frequency). The dielectric is made of quartz to produce a high-density SWP. The SWP source does not require a magnet. The feeding gas and the vacuum pumping system are designed to produce a suitable gas pressure for surface ionization and an effective vacuum environment for accelerated beam transmission.

III. Plasma Design and Simulation

The SWP is a plasma that is excited by propagation of electromagnetic surface waves. SWP sources can be dielectric-bounded [18], [19] (surface waves propagate along the dielectric and plasma interfaces) or metal-bounded [a microwave sheath–voltage combination plasma (MVP) [20] is used, and surface waves propagate along the plasma and sheath interfaces]. In this study, the Maxwell equations and a cold plasma model are used in conjunction with the finite-difference time domain (FDTD) method and COMSOL software to simulate the propagation of surface waves excited by a multicoaxial microwave cable. The effect of different variables, such as the plasma density, the electron collision frequency, and the structure of a hollow circular cylindrical quartz dielectric on the surface wave propagation are separately investigated.

The distributions of the electric fields, electron density, and temperature are designed for uniform and stable system operation based on two principles: the plasma is uniformly distributed in the cavity, and the deposited power is uniformly distributed in the axial direction.

Surface plasmon polaritons (SPPs) [21] for a metal-bounded plasma are introduced to the dielectric-bounded plasma in this study to determine how a plasma is established near a plasma–dielectric interface. SPPs are electromagnetic excitations at the interface between a metal and a dielectric material. The mode changes of a surface wave at the interface between a dielectric and a microwave plasma are also significant for studying SPPs at a dielectric–plasma interface with visible large-scale physical phenomena.

A. Electromagnetic Model for SPPs

The rectangular coordinate system shown in Fig. 2 is adopted to describe the electric field near the dielectric–plasma interface

$$\begin{aligned} E_{x(x,z)} &= A\varepsilon_{x(z)}\, e_{x(x)} \\ E_{z(x,z)} &= A\varepsilon_{z(z)} e_{z(x)} \end{aligned} \tag{1}$$

$$e_{x(x)} = \frac{1}{k_x}\nabla_x \psi_{(x)}, \quad e_{z(x)} = \psi_{(x)} \tag{2}$$

$$\varepsilon_{y(z)} = \frac{1}{k_x}\frac{d\zeta_{(z)}}{dt}, \quad \varepsilon_{z(z)} = \zeta_{(z)}. \tag{3}$$

Substitution of $(k^2 = k_x^2 + k_z^2)$ in (2) and (3) in conjunction with the Helmholtz equation yields

$$\nabla_x^2 + k_x^2 \psi_{(x)} = 0 \tag{4}$$

$$\frac{d^2}{dz^2} - \gamma^2 \zeta_{(z)} = 0 \tag{5}$$

$$\gamma_{p,d} = \mp\sqrt{k_2 - \varepsilon_{p,d} k_0^2} \tag{6}$$

where $\gamma_{p,d}$ is the axial wavenumber; applying the normalization condition results in $\varepsilon_{x(z=-d)} = 1$; following ref. [20], we can use the boundary condition to obtain the axial potential function as follows:

$$\zeta_{(z)} = \begin{cases} \frac{\eta_e}{k_r}\sinh(\gamma z) + \frac{\eta_c}{c_\rho}\cosh(\gamma z) \\ \gamma_d \qquad\qquad D \\ \qquad\qquad c_c \qquad d \end{cases}, \quad \text{for } iz < 0 \tag{7}$$

where $\frac{}{k_r \exp \gamma_p z}$, for $z > 0$

$$D = \frac{\varepsilon_{\gamma_p}}{\varepsilon_p}\cosh(\gamma_d d) - \frac{\gamma_d}{\varepsilon_d}\sinh(\gamma_d d). \tag{8}$$

Combining the above equations with Maxwell's equations yields the solution for the electromagnetic field, where A_1, A_2, and A_3 are constants that depend on the electromagnetic wave amplitude according to the Coulomb specification condition given below

$$A_1 k_x + A_2 k_y = A_3 k_z. \tag{9}$$

For the TM wave model

$$H_z = 0, \quad A_2 = \frac{A_l\, k_y}{k_x} = \frac{Ak_y}{k_x} \tag{10}$$

$$A_3 = Ak_z / k_x. \tag{11}$$

The aforementioned solution reduces to the following electromagnetic field in the dielectric:

$$E_x = \frac{A}{D}\cos(k_x x)\sin k_y \Sigma \Sigma \frac{\gamma_p}{\varepsilon_p}\cosh(\gamma z) + \frac{\gamma_d}{\varepsilon_d}\sinh(\gamma z)$$

$$E_y = \frac{A\, k_y}{D\, k_x}\sin(k_x x)\cos k_y \Sigma \Sigma \frac{\gamma_p}{\varepsilon_p}\cosh(\gamma z) + \frac{\gamma_d}{\varepsilon_d}\sinh(\gamma z)$$

$$E_z = \frac{A}{D}\frac{k^2}{\gamma_d k_x}\sin(k_x x)\sin k_y y \Sigma \frac{\gamma_p}{\varepsilon_p}\sinh(\gamma_d z) + \frac{\gamma_d}{\varepsilon_d}\cosh(\gamma_d z)$$

$$H_x = \frac{A}{i\omega\mu D}\frac{k_y k^2 \varepsilon_d}{k_x \gamma_d}\sin(k_x x)$$

$$\cos k_y \Sigma \Sigma \frac{\gamma_p}{\varepsilon_p}\sinh(\gamma z) + \frac{\gamma_d}{\varepsilon_d}\cosh(\gamma z)$$

$$H_y = -\frac{A}{i\omega\mu D}\frac{\varepsilon_d}{\gamma_d}k_0^2\cos(k_x x)$$

$$\times\sin k_y \Sigma \Sigma \frac{\gamma_p}{\varepsilon_p}\sinh(\gamma_d z) + \frac{\gamma_d}{\varepsilon_d}\cosh(\gamma_d z). \tag{12}$$

The electromagnetic field in the plasma is given by

$$E_x = \frac{A\,\gamma_p}{D\,\varepsilon_p}\cos(k_x x)\sin k_y y \Sigma \exp \gamma_p z \Sigma$$

$$E_y = \frac{A\, k_y \gamma}{D\, k_x \varepsilon_p}\sin(k_y x)\cos k_x y \Sigma \exp \gamma z \tag{13}$$

$$E_z = \frac{z}{D\, k_x \varepsilon_p}\sin(k_x x)\sin k_y y \Sigma \exp \gamma_p z \Sigma$$

$$H_x = \frac{A \quad k}{i\omega\mu\varepsilon_p D\, k_x}{}^{y} k_0^2 \sin(k_x x)\cos k_y y \Sigma \exp \gamma_p z \Sigma$$

$$H_y = \frac{-A}{i\omega\mu\varepsilon_p D}{}^{2} k_0 \cos(k_x x)\sin k_y y \Sigma \exp \gamma_p z \Sigma. \tag{14}$$

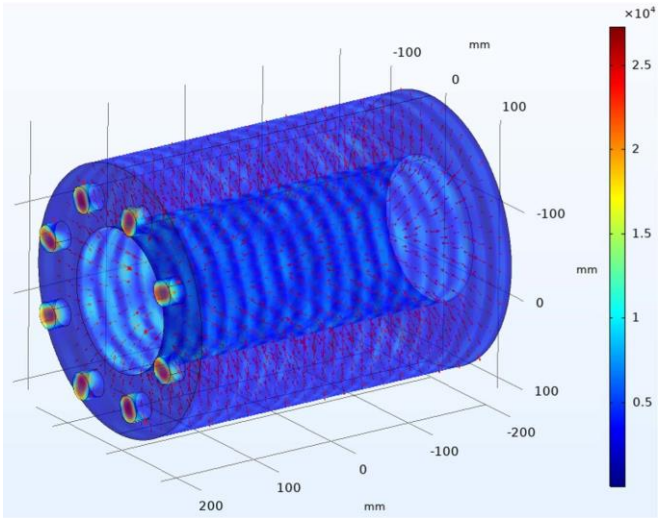

Fig. 3. Microwave transmission simulation results for cylindrical hollow plasma generator (electric field).

Fig. 1 shows the eight coaxial microwave feeding used to supply microwave power to the cylindrical hollow plasma cavity.

The microwave simulation results obtained using the SPP model are presented in Fig. 3. The microwave should move as a stationary wave along the dielectric surface to obtain a sufficiently strong plasma density from SPPs. More details are provided in the description of the plasma simulation results.

B. Numerical Simulation of Plasma

We obtain the following dielectric constant of the plasma for a Drude semi-infinite metal [22] in a vacuum:

$$\varepsilon_p = 1 - \frac{\omega_p^2}{\omega(\omega + iF)} \tag{15}$$

where F denotes the attenuation and the z-component of the electric field is given by

$$E_z = A\sin(k_x x)e^{\alpha z}, \text{ plasma}$$
$$E \quad = B\sin k\, x\, e^{-\beta z} \qquad \text{dielectric} \tag{16}$$

We use $\nabla \times \mathbf{H} = (\partial \mathbf{D}/\partial t)$ to obtain H_y, and the boundary continuity condition $\alpha/\beta = -\varepsilon_m/\varepsilon_d$ to obtain the dispersion relations for the SPPs

$$k_{\text{SPP}} = k_x = \frac{\omega}{c}\sqrt{\frac{\varepsilon_d \varepsilon_p}{\varepsilon_d + \varepsilon_p}} \tag{17}$$

where ε_d is the dielectric constant of the dielectric. The normal component of the electromagnetic field is discontinuous, which results in a surface charge at the boundary of the dielectric ($z > 0$) [21]

$$E_{1z}\,0 \Sigma = -\frac{k_{\text{SPP}}}{k_0 \varepsilon_0 \varepsilon_d} H_0 e^{ik_{\text{SPP}} x} \tag{18}$$

and in the plasma ($z < 0$)

$$E_{2z}\,0 \Sigma = -\frac{k_{\text{SPP}}}{k_0 \varepsilon_0 \varepsilon_p} H_0 e^{ik_{\text{SPP}} x}. \tag{19}$$

Thus, the surface plasma density is given as

$$\rho(x) = \varepsilon_0 (E_{1z} - E_{2z})_{z=0} = \frac{\varepsilon_d - \varepsilon_p}{\sqrt{\varepsilon_d \varepsilon_p (\varepsilon_d + \varepsilon_p)}} H_0 e^{ik_{SPP} x}. \quad (20)$$

It is very difficult to solve Maxwell's equations directly to obtain the electromagnetic fields in the plasma

$$\begin{aligned} \nabla \times \mathbf{E} &= -\frac{\partial \mathbf{B}}{\partial t} \\ \nabla \times \mathbf{B} &= \mu \mathbf{J_p} + \varepsilon\mu \frac{\partial \mathbf{E}}{\partial t} \\ \nabla \cdot \mathbf{D} &= \rho \\ \nabla \cdot \mathbf{B} &= 0. \end{aligned} \quad (21)$$

Thus, we solve Maxwell's equations but use the solution of the magnetic potential ($\underline{A} = \underline{A} e^{iwt}$) to obtain the electromagnetic field. Thus, we obtain

$$j\omega\sigma - \omega^2 \varepsilon \underline{A} + \nabla \times (\mu)^{-1} \nabla \times \underline{A} = J_p. \quad (22)$$

The inverse plasma conductivity is defined as

$$qn_e\sigma^{-1} = \begin{bmatrix} 1 & -\alpha B_z & \alpha B_y \\ \alpha B_z & 1 & -\alpha B_x \\ -\alpha B_y & \alpha B_x & 1 \end{bmatrix} \quad (23)$$

where n_e is the electron number density, $\alpha = (q/(m_e(\nu_e - i\omega)))$, q is the electron charge, m_e is the electron mass, ν_e is the electron-neutral collision frequency, and ω is the angular frequency. The inverse plasma conductivity has a compact form and is therefore convenient to use.

A pair of drift diffusion equations is solved to obtain the electron density and the mean electron energy. Electron convection from fluid flow is neglected. Electron transmission is described by the following equations:

$$\frac{\partial}{\partial t}(n_e) + \nabla \cdot [-n_e(\mu_e \cdot \mathbf{E}) - \mathbf{D}_e \cdot \nabla n_e] = R_e \quad (24)$$

$$\frac{\partial}{\partial t}(n_\varepsilon) + \nabla \cdot [-n_\varepsilon(\mu_\varepsilon \cdot \mathbf{E}) - \mathbf{D}_\varepsilon \cdot \nabla n_\varepsilon] + \mathbf{E} \cdot F_e = R_\varepsilon \quad (25)$$

where the electron source R_ε and the loss of energy due to inelastic collisions are accounted for. The electron mobility can be used to determine the electron diffusivity, the energy mobility, and the energy diffusivity as follows:

$$\mathbf{D}_e = \mu_e T_e, \quad \mu_\varepsilon = \frac{5}{3}\mu_e, \quad \mathbf{D}_\varepsilon = \mu_\varepsilon T_e. \quad (26)$$

The inverse electron mobility can be written in compact form as

$$\mu_e^{-1} = \begin{bmatrix} \frac{1}{\mu_{dc}} & -B_z & B_y \\ B_z & \frac{1}{\mu_{dc}} & -B_x \\ -B_y & B_x & \frac{1}{\mu_{dc}} \end{bmatrix} \quad (27)$$

where μ_{dc} is the electron mobility in the absence of a magnetic field.

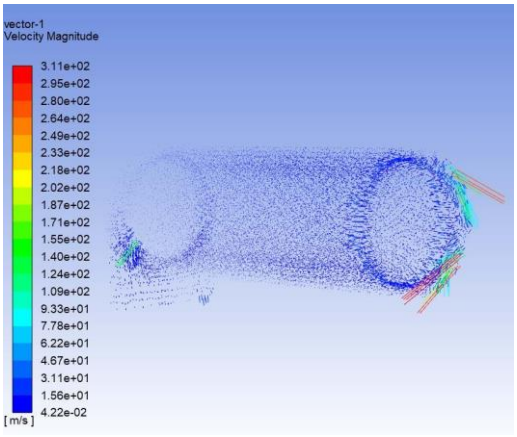

Fig. 4. Velocity of Ar flow in the hollow plasma cavity.

TABLE I
MAIN PROCESSES IN AR PLASMA IONIZATION

No.	Reactions	Description	Δε (eV)
1	$e+Ar \rightarrow e+Ar$	Elastic	0
2	$e+Ar \rightarrow e+Ars$	Excitation	11.5
3	$e+Ars \rightarrow e+Ar$	Superelastic	-11.5
4	$e+Ar \rightarrow 2e+Ar^+$	Ionization	15.8
5	$e+Ars \rightarrow 2e+Ar^+$	Ionization	4.24

Electrons continually gain energy from the electric fields for SPPs at the interface between the dielectric and plasma chambers. The electromagnetic field given by (13) and (15) can be used to express the energy deposition for ignition electrons as

$$P_{SPPs} = \frac{1}{2}\mathrm{Re}\,\mathbf{E} \cdot \mathbf{J}_p^*. \quad (28)$$

The following equation can be solved to obtain the mass fraction of each nonelectron species [23], [24]

$$\rho\frac{\partial}{\partial t}(w_k) + \rho(\mathrm{u} \cdot \nabla)w_k = \nabla \cdot j_k + R_k. \quad (29)$$

The model for argon plasma chemistry involves the following series of collisions, namely elastic, excitation, direct ionization, and stepwise ionization.

IV. RESULTS AND DISCUSSION

To make sure the Ar gas flow have a uniform distribution and completely cover the plasma. Gas flow simulation (by ANSYS 19.0) had conducted before the plasma simulation. In the gas flow simulation, the Ar inflow is set at 70 sccm, and the velocity of Ar flow in the hollow plasma cavity is shown in Fig. 4. With a two-pump system, a uniform gas pressure distribution in the hollow plasma cavity had been got.

The temporal behavior of the simulated electric fields and power deposition, and the corresponding variation in the plasma density and the hot electron temperature up to the steady-state condition are presented in this article. The gas pressure of hydrogen in the plasma chamber is 1 Pa, and

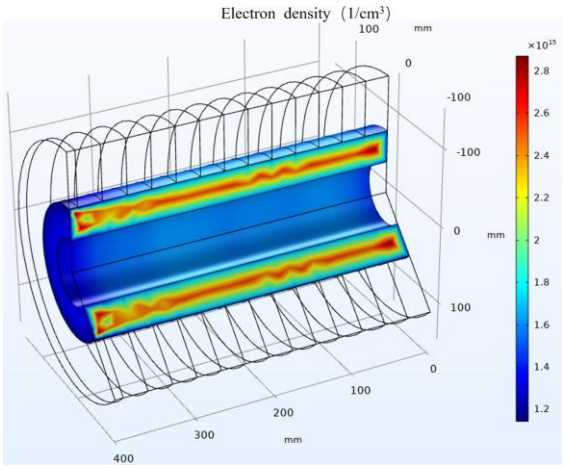

Fig. 5. Simulated plasma density of the cylindrical hollow plasma cavity (2 kW at 1 Pa).

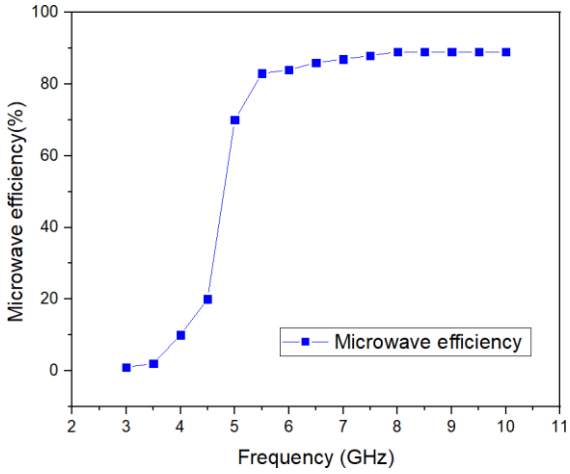

Fig. 6. Microwave efficiency for different microwave frequencies.

the microwave power supplied to the microwave window is 1.5–11 kW. The simulated electron density is shown in Fig. 5.

Prescribed microwaves must be propagated in suitable microwave structures to obtain a high-efficiency plasma cavity. The microwave efficiency for plasma ionization is simulated using different microwave frequencies and cavity structures (by varying the length, radius, and size of the quartz dielectric). The plasma simulation results show that a ∅320 mm × 400 mm plasma cavity with 10-mm-thick ∅300 mm × 400 mm quartz tubular columns optimizes plasma generation and stability. The microwave efficiency is defined as the ratio of the microwave absorption by the plasma to the microwave input.

Fig. 6 shows the microwave efficiency for different microwave frequencies to get the plasma density $2.0 \times 10^{15}/\text{cm}^3$. Considering the price of the microwave power source, 6 GHz is the most suitable frequency for plasma generation. Fig. 7 shows the simulated plasma density at different microwave power levels (using a 6-GHz microwave frequency). A stable and reliable plasma is needed to produce an available wakefield for the accelerator, and plasma uniformity along the axial direction is critical in determining an effective acceleration length. Fig. 8 shows that the fluctuations

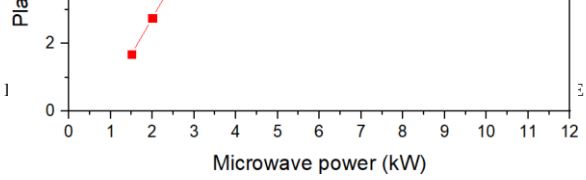

Fig. 7. Simulated plasma density at different microwave power levels.

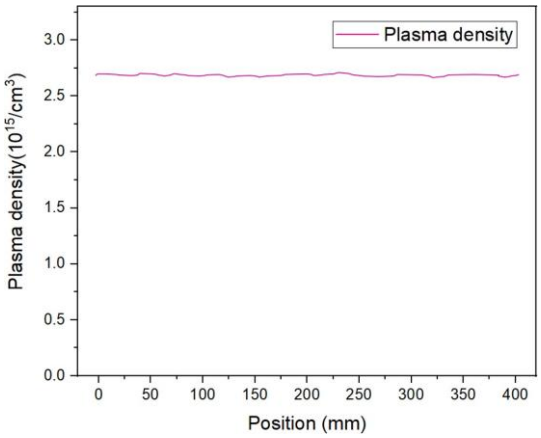

Fig. 8. Plasma density along axial direction (6 GHz at 2 kW).

in the plasma density along the axial direction (6 GHz at 2 kW) are within 2%, which is satisfactory for wakefield acceleration. According to preliminary calculation results, a maximum longitudinal field of 681 MeV/m can be obtained with the plasma density of $2.76 \times 10^{15}/\text{cm}^3$.

V. Conclusion

A cylindrical hollow plasma cavity was designed for a wakefield booster for future e^+e^- colliders. The SWP model was used to optimize the plasma cavity structure, the gas pressure, the microwave frequency, and the microwave power. The simulation results show that 6 GHz at 2 kW microwaves with eight coaxial microwave power feed-ins, a ∅300 mm × 400 mm (length) × 30 mm (thickness) plasma column with a density of $2.76 \times 10^{15}/\text{cm}^3$ can be obtained. The fluctuations in the plasma density are less than 2%, which is satisfactory to provide a long and stable enough region for the wakefield acceleration. In the future, the gas flow simulation will be combined with the plasma simulation to ensure an effective vacuum environment and uniform plasma for the wakefield accelerator. Based on the high stability and reliability cylindrical hollow plasma cavity, a high accelerating gradient with effective acceleration distance more than 400 mm can be expected in the future. Machining of the plasma chamber is in progress. Detailed experimental results of the electron beam

acceleration cavity will be presented in the future. And the wakefield acceleration and transformer ratio optimization will be presented in another article.

ACKNOWLEDGMENT

The authors would like to thank Hefei Comprehensive National Science Center for their strong support. They also expect the STCF to be an important part of the science center.

REFERENCES

[1] Q. Luo, W. Gao, J. Lan, W. Li, and D. Xu, "Progress of conceptual study for the accelerators of a 2-7 GeV super tau charm facility at China," in *Proc. 10th Int. Particle Accel. Conf.(IPAC)*, 2019, pp. 643–645.

[2] *Positron White Paper*. [Online]. Available: http://www.slac.stanford.edu/econf/C010630/papers/E3006.PDF

[3] I. Blumenfeld *et al.*, "Energy doubling of 42 GeV electrons in a metre-scale plasma wakefield accelerator," *Nature*, vol. 445, no. 7129, pp. 741–744, Feb. 2007.

[4] S. Gessner *et al.*, "Demonstration of a positron beam-driven hollow channel plasma wakefield accelerator," *Nature Commun.*, vol. 7, no. 1, p. 11785, Sep. 2016.

[5] T. Katsouleas *et al.*, "Laser wakefield acceleration & optical guiding in a hollow plasma channel," in *Proc. AIP Conf.*, 1992, pp. 480–489.

[6] S. Lee, T. Katsouleas, R. Hemker, E. Dodd, and W. Mori, "Plasma-wakefield acceleration of a positron beam," *Phys. Rev. E, Stat. Phys. Plasmas Fluids Relat. Interdiscip. Top.*, vol. 64, no. 4, 2001, Art. no. 045501.

[7] C. Schroeder, C. Benedetti, E. Esarey, and W. P. Leemans, "Laser-plasma-based linear collider using hollow plasma channels," *Nucl. Instrum. Methods Phys. Res. A, Accel. Spectrom. Detect. Assoc. Equip.*, vol. 829, pp. 113–116, Sep. 2016.

[8] T. Chiou *et al.*, "Laser wake-field acceleration and optical guiding in a hollow plasma channel," *Phys. Plasmas*, vol. 2, no. 1, pp. 310–318, 1995.

[9] G. Shvets, J. S. Wurtele, T. C. Chiou, and T. C. Katsouleas, "Excitation of accelerating wakefields in inhomogeneous plasmas," *IEEE Trans. Plasma Sci.*, vol. 24, no. 2, pp. 351–362, Apr. 1996.

[10] C. B. Schroeder, E. Esarey, C. Benedetti, and W. P. Leemans, "Control of focusing forces and emittances in plasma-based accelerators using near-hollow plasma channels," *Phys. Plasmas*, vol. 20, no. 8, Aug. 2013, Art. no. 080701.

[11] T. C. Chiou and T. Katsouleas, "High beam quality and efficiency in plasma-based accelerators," *Phys. Rev. Lett.*, vol. 81, no. 16, pp. 3411–3414, Oct. 1998.

[12] C. Schroeder, D. Whittum, and J. Wurtele, "Multimode analysis of the hollow plasma channel wakefield accelerator," *Phys. Rev. Lett.*, vol. 82, no. 6, p. 1177, 1999.

[13] W. Kimura, H. Milchberg, P. Muggli, X. Li, and W. B. Mori, "Hollow plasma channel for positron plasma wakefield acceleration," *Phys. Rev. Special Topics-Accel. Beams*, vol. 14, no. 4, 2011, Art. no. 041301.

[14] L. Yi *et al.*, "Scheme for proton-driven plasma-wakefield acceleration of positively charged particles in a hollow plasma channel," *Phys. Rev. Special Topics-Accel. Beams*, vol. 16, no. 7, Jul. 2013, Art. no. 07130119.

[15] L. Yi *et al.*, "Positron acceleration in a hollow plasma channel up to TeV regime," *Sci. Rep.*, vol. 4, no. 1, p. 4171, May 2015.

[16] C. A. Lindstrøm *et al.*, "Measurement of transverse wakefields induced by a misaligned positron bunch in a hollow channel plasma accelerator," *Phys. Rev. Lett.*, vol. 120, no. 12, Mar. 2018, Art. no. 124802.

[17] H. Kousaka and K. Ono, "Fine structure of the electromagnetic fields formed by backward surface waves in an azimuthally symmetric surface wave-excited plasma source," *Plasma Sources Sci. Technol.*, vol. 12, no. 2, p. 273, 2003.

[18] S. Kar, L. Alberts, and H. Kousaka, "Microwave power coupling in a surface wave excited plasma," *AIP Adv.*, vol. 5, no. 1, Jan. 2015, Art. no. 017104.

[19] M. Nagatsu *et al.*, "Low-temperature sterilization of wrapped medical instruments using low-pressure microwave plasma produced by face-type planar launchers," in *Proc. 28th ICPIG*, 2007, pp. 1395–1396.

[20] X. Deng, H. Kousaka, T. Tokoroyama, and N. Umehara, "Thermal stability and high-temperature tribological properties of a-C:H and Si-DLC deposited by microwave sheath voltage combination plasma," *Tribol. Online*, vol. 8, no. 4, pp. 257–264, 2013.

[21] J. M. Pitarke, V. M. Silkin, E. V. Chulkov, and P. M. Echenique, "Theory of surface plasmons and surface-plasmon polaritons," *Rep. Prog. Phys.*, vol. 70, no. 1, pp. 1–87, Jan. 2007.

[22] J. J. Miret, C. J. Zapata-Rodríguez, Z. Jaksic, S. Vukovic, and M. R. Belic, "Substantial enlargement of angular existence range for dyakonov-like surface waves at semi-infinite metal-dielectric superlattice," *J. Nanophotonics*, vol. 6, no. 1, Nov. 2012, Art. no. 063525.

[23] A. Jüngel and Y. J. Peng, "A hierarchy of hydrodynamic models for plasmas. Quasi-neutral limits in the drift-diffusion equations," *Asymptotic Anal.*, vol. 28, no. 1, pp. 49–73, 2001.

[24] D. Vasileska, "Drift-diffusion model: Introduction," Associate Professor, Arizona State Univ., Tempe, AZ, USA. [Online]. Available: https://nanohub.org/resources/1545/download/ddmodelintroductorypartword.pdf

Q. Luo (Member, IEEE) received the Ph.D. degree from the National Synchrotron Radiation Laboratory (NSRL), University of Science and Technology of China (USTC), Hefei, China, in 2009, where he conducted theoretical and experimental research on accelerator beam measurements using resonant cavities.

From 2009 to 2017, he was a Scientist at NSRL, USTC. He led the developments and construction of accelerator magnets for Hefei Light Source II from 2012 to 2014, and worked as a Team Leader of accelerator physics for preliminary conceptual design at the Hefei Advanced Light Facility from 2014 to 2016. He is currently an Associate Professor with the School of Nuclear Science and Technology (SNST) and NSRL, USTC. His current research interests include accelerator facility design, beam physics and diagnostics, and the design and application of accelerator-based scientific equipment. Recently, he leads the accelerator division of conceptual design at the Super Tau Charm Facility, a 2–7 GeV circular electron–positron collider, which would be a successor of Beijing Electron Positron Collider II.

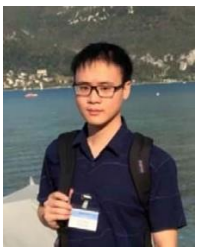

A. L. Zhang received the Ph.D. degree from the University of Chinese Academy of Sciences, Beijing, China, in 2017, where he conducted the design and experimental research on high-intensity dc proton permanent magnet 2.45 GHz ECR ion source for CADS project.

From 2017 to 2019, he was with the Center National de la Recherche Scientifique (CNRS), Paris, France, where he is mainly concentrated on the design of the new prototype of the FEBIAD type ion source IRENA3 for ISOL method. He is currently a Deputy Researcher with the School of Physical Sciences, University of Science and Technology of China, Hefei, China. His current research interests include the future e^+e^- collider design, ion source, plasma simulation, and the plasma–wakefield acceleration. Most recently, his research has been focused on a cylindrical hollow plasma cavity for wakefield booster for future e^+e^- colliders.

H. P. Peng received the Ph.D. degree from the School of Physical Sciences, University of Science and Technology of China (USTC), Hefei, China, in 2004, where he conducted the BESII data analysis and BESIII detector research and development work.

From 2004 to 2007, he held a post-doctoral position at the Deutsches Elektronen-Synchrotron (DESY), Hamburg, Germany. He participated in H1 data analysis and online/offline data monitoring software development, using ep data to study the generation mechanism of charm quarks. From 2007 to 2011, he was a Research Associate with the University of Wisconsin–Madison, Madison, WI, USA. He participated in the ATLAS experiment, mainly engaged in ATLAS high-energy JET energy calibration and simulation research, as well as the search for new physics and new peculiar states. He is currently a Professor with the School of Physical Sciences, USTC. His current research interests include future electron–positron collider design, detector design, and the search for new physics beyond the standard model. Recently, he leads the Super Tau Charm Facility in China, a 2–7 GeV circular electron–positron collider.